Weierstraß-Institut
für Angewandte Analysis und Stochastik

im Forschungsverbund Berlin e.V.

Improving the modulation bandwidth in semiconductor lasers by passive feedback

Mindaugas Radziunas[1] , Annegret Glitzky[1] , Uwe Bandelow[1] ,

Matthias Wolfrum[1] , Ute Troppenz[2] , Jochen Kreissl[2] ,

Wolfgang Rehbein[2]

submitted: 3 July 2006

[1] Weierstraß-Institut
    für Angewandte Analysis und Stochastik
    Mohrenstrasse 39
    D – 10117 Berlin
    Germany
    E-Mail: radziuna@wias-berlin.de,
            glitzky@wias-berlin.de,
            bandelow@wias-berlin.de,
            wolfrum@wias-berlin.de

[2] Fraunhofer-Institut für Nachrichtentechnik
    Heinrich-Hertz-Institut
    Einsteinufer 37
    D – 10587 Berlin
    Germany
    E-Mail: troppenz@hhi.fraunhofer.de,
            kreissl@hhi.fraunhofer.de,
            rehbein@hhi.fraunhofer.de

No. 1149
Berlin 2006

W I A S

Abstract

We explore the concept of passive-feedback lasers for direct signal modulation at 40 Gbit/s. Based on numerical simulation and bifurcation analysis, we explain the main mechanisms in these devices which are crucial for modulation at high speed. The predicted effects are demonstrated experimentally by means of correspondingly designed devices. In particular a significant improvement of the modulation bandwidth at low injection currents can be demonstrated.

1 Introduction

Directly modulated semiconductor lasers are of great interest for low cost transmitter applications in short reach and very short reach optical data transmission systems. Mainly single section DFB laser modules are considered for this purpose. However, until now, the system application of these lasers for data rates beyond 10 Gbit/s per channel is limited by the modulation bandwidth (MBW), which is related to the relatively slow carrier-photon (CP) interaction as it appears in the relaxation-oscillation of such lasers.

There exist a few concepts allowing to increase MBW - and there is hope that they allow for an increase of the large signal direct modulation rate as well. One of the techniques to increase the CP resonance frequency is the optimization of the laser design and of the composition of the heterostructure material [1]. The experimental realization and transition experiments for a 40 Gbit/s data stream are reported in [2, 3, 4]. An extinction (ratio of the maximal and the minimal field intensities) of about 4 to 5 dB has been achieved. Using the single section concept [4], the main challenge seems to be the handling of very short laser lengths and to avoid the oxidation of the required Al-containing layers.

Another approach is based on optical injection locking [5]. In this case, the MBW can be tuned according to the wavelength-detuning of a master laser relatively to a slave laser. This technique allows to increase the main resonance frequency of the slave laser up to 50 GHz. However, to our knowledge, an appropriate performance of such a laser system under large signal modulation with high bit rate has not yet been reported.

As third, a multi-section laser concept has been used by several authors. An experimentally observed increase of the 3 dB MBW up to about 40 Gbit/s for various multi-section laser structures has been shown e.g. in [6, 7, 8]. The main reason

for the MBW enhancement in all these cases was the resonance between two spectrally neighboured longitudinal modes of the compound laser cavity [8, 9, 10]. Here, instead of trying to push the MBW by an increased CP resonance frequency, the authors have exploited an additional photon-photon (PP) resonance peak at frequencies which potentially exceed the usual CP frequency a few times. Under certain conditions, this PP resonance is known to become even undamped and to result in Mode-Beating pulsations [11, 12, 13, 14].

In this paper, we also follow the multi-section laser concept and elucidate its potential for high speed direct modulation. In a first step, we have investigated theoretically the performance of different laser types: DBR lasers, as in [10], two-section distributed feedback (DFB) lasers as in [9, 12], a Coupled Cavity Injection Grating laser as in [8], an Active Feedback Laser as in [13, 14] and a Passive Feedback Laser (PFL) as considered in [11, 13]. In general, we could find the PP resonance and an increased MBW in all these laser structures. In order to keep the device structure as simple as possible, and to achieve a better understanding of the mechanisms governing the laser dynamics under direct current modulation, we analyzed theoretically and experimentally the behaviour of the simple PFL depicted schematically in Fig. 1. This device consists of two adjacent monolithically integrated sections: the active single-mode index-coupled DFB section and the integrated feedback (IFB) section with a high reflection coated facet. The latter has to provide a sufficiently strong delayed optical feedback to the DFB section. Note also, that a high reflection coating of the IFB section edge increases the efficiency of the laser device, because light is emitted only from one laser facet at the DFB section.
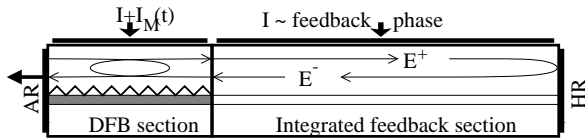

Figure 1: Scheme of a PFL, consisting of an anti-reflection coated DFB- and a high-reflection coated Integrated Feedback section.

This paper continues our theoretical study in [15] by completing it with novel experimental and theoretical results. It is organized as follows. In section 2 we start with a short introduction of the mathematical model and the software tools, which we use for simulation and analysis of multi-section semiconductor lasers. Next, we perform a detailed bifurcation and small signal response analysis of a typical PFL with high field feedback from the IFB section. In section 3 we report some experimental results for the devices, which have been realized following the theoretical suggestions. In particular, the operation conditions for a MBW enhancement up to 30 GHz are described. The agreement of these experimental results and theoretical predictions will be discussed. Further theoretical predictions for the performance of the device under large signal current modulation are presented in section 4. Finally, our conclusions are drawn in section 5.

2   Modeling and analysis of the PFL

2.1   Model of the PFL

For simulation of the dynamics of multi-section lasers we use the Traveling Wave (TW) model [16]. This model describes the spatio-temporal evolution of slowly vary-ing envelopes of counter-propagating optical fields, which are nonlinearly coupled to the spatially averaged carrier density within the DFB section. For simulations of the TW model we used the software package `LDSL-tool` [17].

Table 1: Parameters used in simulations

DFB section parameters		
length of the section	l	$250\,\mu$m
internal field loss	α	$20/$cm
linewidth enhancement factor	α_H	-4
transparency density	n_{tr}	$10^{24}/$m^3
field coupling factor	κ	$130/$cm
cross section area of the active zone	σ	$65\cdot10^{-15}$ m^2
current injection	I	60mA
recombination coefficient	$1/\tau$	$0.2/$ns
recombination coefficient	B	10^{-16}m$^3/$s
recombination coefficient	C	$1.3\cdot10^{-41}$m$^6/$s
Lorentzian gain dispersion peak position	$\bar{\omega}$	~ 5nm
gain dispersion width at half maximum	$\bar{\gamma}$	~ 60nm
gain dispersion height	$\bar{g}$	$200/$cm
IFB section parameters		
length of the section	l	$300\,\mu$m
internal field loss	α	$15/$cm
IFB section facet reflectivity	R	0.99

In our simulations we have assumed a central wavelength $\lambda_0 = 1.57\,\mu$m, a group index $n_g = 3.6$ and the sectional parameters as listed in Table 1. Moreover, we have used no additional wavelength detuning or nonlinear gain compression and have assumed an anti-reflection coating of the DFB section facet. A detailed explanation of all these parameters can be found in, e.g., [16, 18].

The impact of the IFB section depends on its length l_{IFB}, the field feedback strength K and the field phase shift φ:

$$K = R \cdot \exp(2l_{IFB}\alpha_{IFB}), \qquad\qquad \varphi = 2\pi\frac{2l_{IFB}n_{IFB}^{eff}}{\lambda_0}.$$

The phase shift can be controlled via the refractive index n_{IFB}^{eff} by the injection

current I_{IFB} into the IFB section.[1] A proper selection of the IFB section length should guarantee an effective tunability of φ as well as a proper mode frequency separation of the compound-cavity modes, which is proportional to the PP resonance frequency. In order to obtain a high optical feedback strength K we use a high-reflection (HR) coating of the IFB section facet.

2.2 Linear stability analysis

For better insight along with simulations of the TW model we also used certain mode approximation systems. These systems properly approximate the dynamics of the full TW model on finite-dimensional exponentially attracting invariant manifolds, see [19], the dimensionality of which decides for the number of modes which have to be taken into account. For the purposes of this paper we used 5 modes, and the resulting 5 mode approximation system then consists of 10 ordinary differential equations. This is a substantial simplification with respect to the original TW system and enabled us to perform a numerical bifurcation analysis by path following methods [18]. In this way we obtained the location of the continuous wave (cw) states in the parameter space, their linear stability properties, and their small signal modulation response.
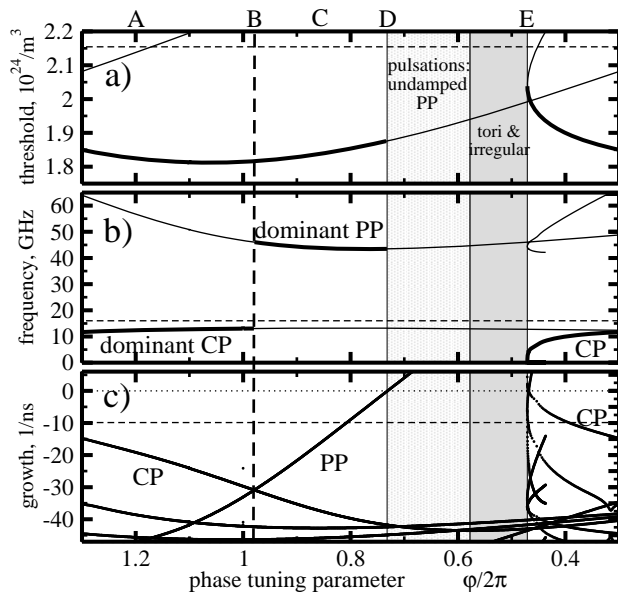

Figure 2: Bifurcation diagram. Threshold density of the cw states (a), main resonance frequencies of the dominant state (b), and the corresponding growth (negative damping) of these resonances (c). Thin dashed: corresponding values in the solitary DFB laser. Thick and thin solid: stable and unstable cw states (a), frequency of the main and the side resonances (b). Shadings: parameter intervals where stable periodic orbit (undamped PP resonance) and quasiperiodic or irregular behaviour are only accessible in simulations.

The one-parameter bifurcation diagram in Fig. 2 is a typical example for such a study. Panel (a) shows the dependence of the cw state threshold on the phase parameter φ along which everything is 2π-periodic. Within the white area we have a stable cw state. At the phase A the CP resonance is dominant. This situation is comparable to the solitary DFB laser (see thin dashed lines in Fig. 2), but the

---

[1]In practice, I_{IFB} causes also free carrier absorption, which we neglect here to concentrate on the essential effects.

threshold is reduced due the light re-injection into the DFB section from the IFB section side. At the phase B both CP and PP resonances are equally supported. This is not possible in the solitary laser, since this PP resonance occurs due to interaction of the neighbouring compound cavity modes determined by both, DFB and IFB sections. At the phase C this PP resonance dominates and the CP resonance is suppressed. At the phase D the PP resonance becomes undamped which will result in mode-beating pulsations. Later on, a pair of an unstable saddle-type and a stable cw state originates at the phase E. The main resonance of this stable cw state is of CP type. Due to periodicity with respect to the phase parameter, the cw states at the right edge of Fig. 2 are identical to those at the left side of these diagrams.

The panel (c) of Fig. 2 demonstrates the constructive or destructive impact of the field feedback from the IFB section. Comparison of thick solid (two-section laser) and thin dashed (solitary DFB laser) lines shows that at $\sim$60% of all possible feedback phases the damping of the main cw state is improved.

2.3   Modulation performance of PFL

At the phases A, B and C from Fig. 2 we have performed a small signal analysis numerically. We modulated the injection I_{DFB} with a small harmonic signal of frequency f. Then, we recorded the amplitude of the periodic response by numerical path-following of the resulting periodic solution: see [18], where a similar procedure was described. The normalized optical response of the laser to the small amplitude modulation is represented in Fig. 3.
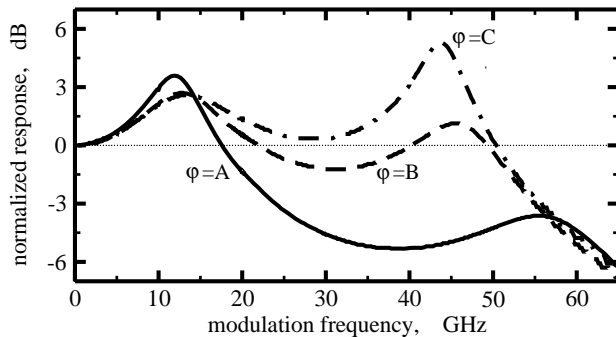

Figure 3: Small signal analysis, performed at three different phase parameter values.

This figure compares the laser performance at the phases A, B and C, showing the strong suppression of the PP resonance at A, and the enhancement of this resonance at B and C. This figure demonstrates also the increase of the 3 dB MBW with the enhancement of the PP resonance. Note also that the resonance frequencies and their relative damping are in agreement with our linear stability analysis of the cw state performed in Fig. 2b,c.

We checked also, how Fig. 2 changes under the change of some basic parameters described above. We have found that in order to get a dominance of the PP resonance, one needs a high feedback strength K, which depends on the field loss within the

IFB section, at the facet of the IFB section, and at the interface of both sections. Higher values of differential gain and steeper power-current characteristics are also useful to achieve a better device performance under large signal modulation.

3 Experimental findings

3.1 Device

We have realized PFL-structures consisting of a DFB laser and an integrated passive feedback section. The laser section within the two-section device is based on a ridge waveguide design. The active region consists of $In_{1-x}Ga_xAs_{1-y}P_y$ strained layer multi-quantum wells (MQWs) embedded between asymmetric (1.18 μm/1.3 μm) quaternary waveguides. A rectangular grating was etched into the upper waveguide by reactive ion etching. After grating definition, the upper waveguide and the MQW-layers in the IFB phase tuning section are removed and in a regrowth step the p-cladding layers are grown. The index coupling coefficient κ of the DFB grating lies in the region between 130/cm and 170/cm. For both, the DFB and the phase sections, the length varies between 250 μm and 300 μm.
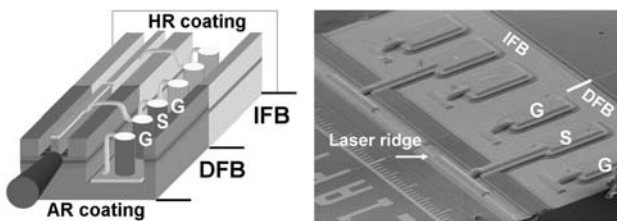

Figure 4: PFL scheme (left) and scanning electron microscope picture (right) of the fabricated device. The output facet of the DFB section is AR coated and the rear facet of the phase section is covered with a HR coating (reflectivity > 95 %).

The fabrication process is completed by the contact formation. To avoid parasitic capacities we minimized the contact areas.

The capacity of the structure determined by $s -$ parameter measurements is 0.5 pF what implies a radio frequency (RF) cutoff frequency beyond the required 40 GHz (R = 6 Ω). The pad geometry allows the application of standard microwave probe heads for measurements at bar level.

3.2 Measurement setup

The device characterization has been performed on chip level, where a dc needle was used for injection of current into the phase section and a Ground Signal Ground (GSG) microwave probe provided modulation and dc biasing for the DFB laser section. The dc driving and the RF power supplied by a sweep generator have been combined through a bias-T. The PFL output was coupled to a lensed fiber from where it was passed to several measurement instruments including a 40 GHz

photodetector combined with an RF-spectrum analyzer for monitoring the electrical power spectrum as well as an optical spectrum analyzer for optical spectrum monitoring.

3.3   Verification of high frequency PP resonances

We started our investigations under dc-biasing of both the phase section and the DFB section. The aim was to prove first the theoretical predictions on the dominance of PP resonance under certain feedback conditions and to identify in a second step the feedback phase conditions for high MBW. In the experiment the change of feedback phase can be easily achieved by modifying the phase current I_{IFB}. The increase of carrier density at moderate currents can provide a 2π phase rotation even for short IFB sections down to 200 μm.
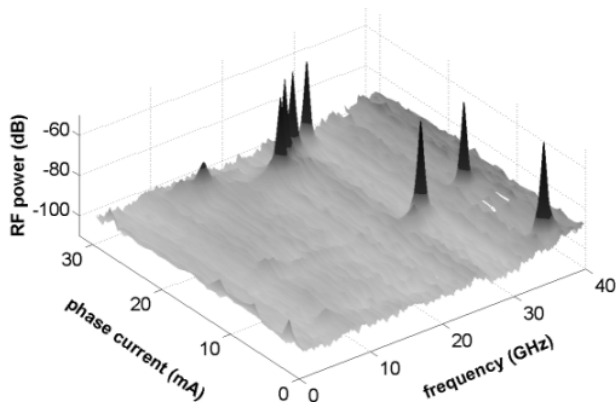

Figure 5: RF spectra of PFL structure in dependence on phase current; $I_{DFB} = 60$ mA, step of phase current change: 1 mA. The spike like appearance of PP resonances is due the digital step width of phase current.

We restricted our investigations to those devices which show a stable single mode operation accomplished by a side mode suppression ratio of higher than 35 dB, where no hopping between different stopband side modes has been found under the influence of changing feedback phase. For the investigated PFL structures we observed a typical behaviour of the RF power spectra when the phase current is increased (Fig. 5). In a large range of phase current we found stationary laser operation with low amplitude noise. These regions of stationary states are separated by phase current regions where the laser operates in a non-stationary regime. The latter is characterized by strong pulsations with frequencies of 25 to 40 GHz, indicating the occurrence of theoretically predicted high frequency mode-beating oscillations. Under zero phase current the laser structure investigated here operates in a non-stationary regime with a pulsation frequency of about 38 GHz. Similar phase conditions reappear at phase currents around 12 and 28 mA. It is visible, that from period to period the pulsation frequency decreases. This can be explained by a reduced feedback strength resulting from carrier induced waveguide losses. Within the same phase period the pulsation frequency increases with phase current.

Summarizing the dc biasing characteristics, we observe regions of mode-beating oscillations in our PFL structure which are expected from the simulations. In addition,

the experimentally determined mode-beating oscillations meet the frequency range, which is needed for a MBW enhancement.

3.4 Modulation bandwidth under feedback

We focus now on the identification of stationary operation regimes offering a high modulation speed of the laser by low damped PP resonances. Following the theoretical results, these states are supposed to occur at phase currents just below the onset of PP self-oscillations. We investigated the properties of our PFL structures under small signal current modulation and compared the results with the dynamic properties of the laser under dc biasing in the following way: We operated the DFB-section at different fixed bias currents and recorded the optical spectrum, the RF spectrum, and the modulation response under increasing phase current. Fig. 6 summarizes the experimental observations for a PFL-structure with a 250 μm DFB section ($\kappa =$ 170/cm) and a 250 μm IFB section. The area plots in the first row illustrate how the spectra are influenced by the phase current. The second row shows the respective spectra for selected operation points.
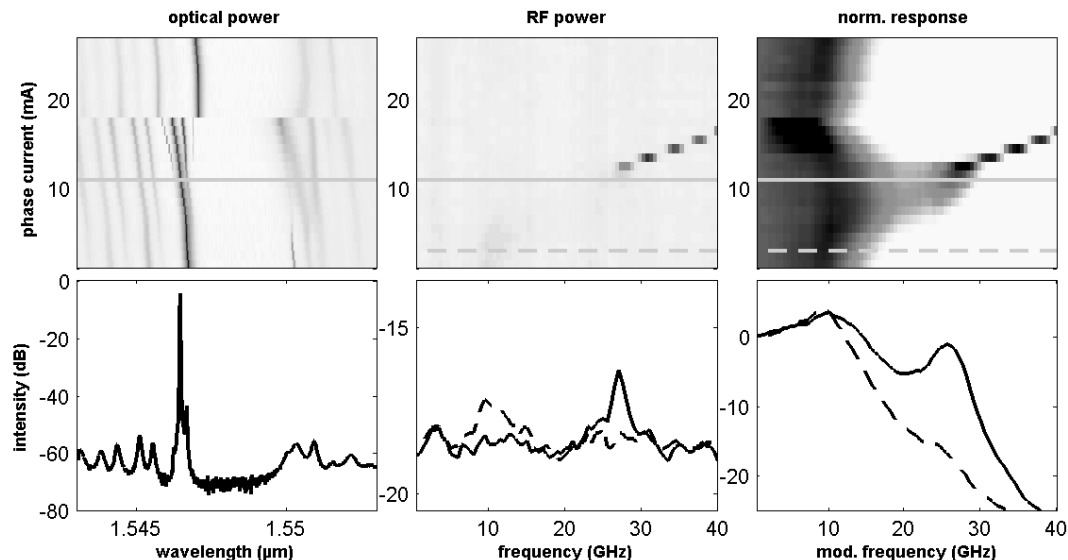

Figure 6: Tuning of the MBW in PFL structure (DFB: 40 mA). First row: optical spectra, RF power spectra and normalized response on small signal current modulation under variation of phase current from 0 to 27 mA. Second row: selected line plots at phase currents of 4 mA and 11 mA.

The investigated range of phase current from 0 to 27 mA shown in the first row of Fig. 6 represents a phase rotation of almost 2π. A non-stationary operation of the laser due to undamping of the PP resonance at frequencies from 28 to 40 GHz is found for phase currents of 13 to 18 mA: see middle part of Fig. 6. Stationary states characterized by the absence of strong RF power amplitudes are found for all other investigated currents. In the optical spectra on the left side these observations are

confirmed. The spectra reveal a stable single mode emission in the stationary state (phase current 0–12 mA, 18–27 mA) with a dominant mode at the shorter wavelength side of the stopband. On the other hand, a typical mode beating spectrum with two main peaks is observed for the non-stationary states. It has to be noted that the optical spectra show an increase of the peak separation with increasing phase current. This finding coincides well with the observed increase of the PP frequencies in the RF power spectra. Measurements of the small signal modulation response are shown on the right hand side of Fig. 6, where the response to the modulation frequency is normalized to the value measured at low frequencies (0.5 GHz). The white areas indicate a modulation response which has been dropped down by more than 3 dB. The figure reveals clearly the change of MBW under changed feedback conditions. At zero phase current the MBW of the PFL is limited to about 12 GHz which is already higher than the 8 GHz MBW of a comparable solitary laser without any feedback. The increase of phase current from 0 to 12 mA is accompanied by an enhancement of the 3 dB MBW up to 29 GHz. Higher phase currents will not further improve the MBW, since the regions of self oscillations are not suited for direct laser modulation.

The line plots in the second row illustrate this scenario in more detail. A 4 mA phase current stands for phase conditions with dominant CP oscillations. Both the RF power spectra and the modulation response exhibit maxima at around 10 GHz. This situation is changed at a phase current of 11 mA. Here, the spectra reflect the moderately damped PP resonances leading to a high small signal MBW and hence optimum feedback conditions. It has to be noted that this high MBW is achieved for a comparably small DFB current of 40 mA. This fact underlines the potential of the PFL concept for direct signal modulation.

3.5 Discussion

The experimental results discussed above reproduce the essential predictions from the simulation studies described in Section II: (i) the PP resonances occur in the predicted operation regions of the laser, (ii) in proper operation regions the MBW could be strongly improved by the PP resonance (maximum 3 dB MBW of about 30GHz), and (iii) the essential parameter for adjusting the proper operation point is the phase current in the IFB section.

For the application in communication systems the modulation response should not only have a high bandwidth but also a flat characteristic. Further optimization of the device will be necessary to get a balanced damping of both the CP and the PP resonances.

Some deviations from the theoretical predictions occur for the frequency and damping behaviour of the CP resonances given in the one-parameter bifurcation diagram of Fig. 2 between phase point A and C. In the experiments the CP frequencies are more phase-dependent and the damping shows not the predicted linear increase there. The reason for this deviation seems to be the difference between the strong

9

feedback scenario in our modeling assumptions and the unknown feedback strength in the realized devices, which might be smaller because of higher losses in the IFB section and lower facet reflectivity. Regarding this point, the theoretical predictions indicate a potential for a better performance, which can be realized by further optimization of the device.

4   Outlook on large signal analysis

The final goal of our study is to build laser devices for converting large amplitude 40 Gbit/s electrical signals into optical ones. Thus, we are not restricting our study to the already demonstrated improvement of the MBW, but also perform numerical simulations with strongly modulated current injection. For this reason, we investigate first how fast changes of the applied current at the contacts of the laser can be translated into its active zone.
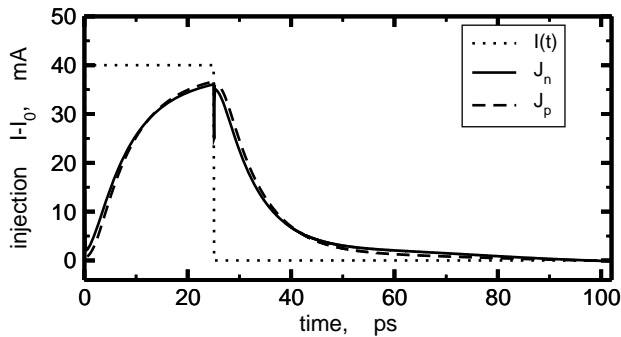

Figure 7: Transients of large-signal current modulation, calculated with `WIAS-TeSCA`. Dotted: rectangular injection current pulse $I(t)$ at the metal contact. Thick lines: electron- (J_n, full line) and hole current (J_p, dashed) injected into the active zone.

For this purpose we have studied the impact of carrier transport along a transverse cross section of the laser in addition, by using our Drift-Diffusion based simulator `WIAS-TeSCA` [20] as sketched e.g. in [21]. In such a transverse cross section we solved the transport equations for electrons and holes coupled to the Poisson equation for the electrostatic potential. The current densities are driven by gradients of the quasi-Fermi potentials, which are linked with the carrier densities by means of Fermi-Dirac statistics. Optical waveguiding is taken into account by corresponding Helmholtz equations for different transverse modes of the optical field. This model is selfconsistently closed by corresponding photon balance equations which balance the optical intensity of the transverse modes, see [21]. The latter implicitly assumes a photon flow through a longitudinal homogeneous laser, such that this model cannot resolve fully our longitudinal sectioned device. Nevertheless it resolves in detail the injection of carriers into the active region, even under conditions of large signal current modulation as we sketch in Fig. 7.

There, we calculated the proportion of the injection current I entering the metal contact of the device to the current J_n and J_p which enters the active zone, for the large signal current modulation regime. The net current J_n of the electrons and J_p of the holes into the active zone has been calculated by the integral of the

10

divergence of electron and hole current density over the active region in each time step, respectively.

The conditions for simulation of the large-signal current modulation have been the following. At some fixed operating point I_0 we added a short rectangular current pulse, such that the injection $I(t)$ is given by

$$I(t) = \begin{cases} I_1, & \text{if} \quad 0 < t < T \\ I_0, & \text{if} \quad t > T. \end{cases}$$

We choose $T = 25$ ps, corresponding to the 40 GHz period of the non-return to zero (NRZ) pseudo random bit sequence (PRBS) signal. Fig. 7 directly compares the behaviour of J_n and J_p for RW laser during and after the pulse. J_n and J_p show a shark fin behaviour with a reduced modulation depth and a delay compared to $I(t)$. The calculations show that J_n and J_p are nearly the same. This confirms the assumption $n = p$ for undoped active regions, which is fundamental for all rate equation models using a single carrier species. This assumption is also used in our simulation package `LDSL-tool` and it is remarkable that it still holds under conditions of 40 GHz large-signal modulation. As a practical result, the simulations with `WIAS-TeSCA` delivered specific suggestions on the realistic injection current transfer into the active zone.

Based on that, we perform simulations with our longitudinal TW model `LDSL-tool` under large signal injection current modulation with 40 Gbit/s NRZ PRBS signals. According to the suggestion of Fig. 7, we replace each rectangular pulse of $I(t)$ in the NRZ signal sequence by

$$\tilde{I}(t) = \begin{cases} I_1 + (\tilde{I}(0) - I_1)e^{-\gamma_1 t}, & \text{if} \quad I(t) = I_1 \text{ at } 0 < t < T \\ I_0 + (\tilde{I}(0) - I_0)e^{-\gamma_0 t}, & \text{if} \quad I(t) = I_0 \text{ at } 0 < t < T \end{cases}.$$

Here, I_1 and I_0 are the expected injection values at the active zone for constant signals "1" or "0", respectively. The exponential transition factors γ_0 and γ_1 fit to Fig. 7.
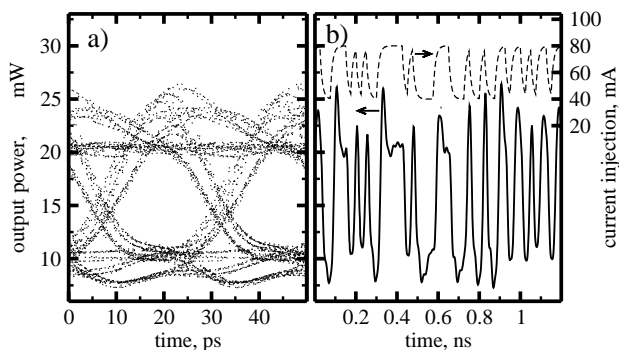

Figure 8: Simulated response of the device to a $(2^7\text{-}1)$ PRBS current modulation (NRZ). a): eye diagram. b): injected current (dashed), field output (solid).

In particular, we chose the feedback phase C (see Fig. 2) and perform the simulation with randomly modulated current $\tilde{I}_{DBF}(t)$ at 40 Gbit/s rate. The obtained laser response is presented in Fig. 8 and shows clearly opened eyes with an extinction meeting the minimum requirements for system applications. The overshootings of

11

the field intensities lead to a broadening of the upper part of the eye diagram and corresponding spikes in panel (b). Obviously, they result from a too moderate damping of the nearby PP resonance and the eye diagram can be further improved by a higher frequency of the dominant PP resonance as well as higher damping of both CP and PP resonances.

5   Conclusion

The concept of passive feedback lasers (PFL) has been used successfully for high speed direct signal modulation. Our theoretical investigations show that the optical feedback can improve the modulation properties of the laser by inducing a photon-photon (PP) resonance close to the desired frequency of 40 GHz and, at the same time, suppressing the usually observed slower relaxation oscillations.

These theoretically predicted effects have been demonstrated experimentally by realizing correspondingly designed devices. They showed the existence of the PP resonance, leading to a significant enhancement of the small signal modulation bandwidth. The corresponding operation conditions can be tuned efficiently by the injection current to the integrated feedback section.

The potential for large signal modulation has been explored by numerical simulations, showing open eye diagrams at 40 Gbit/s NRZ-PRBS current modulation.

Acknowledgment

References

[1] M. N. Akram, Ch. Silfvenius, O. Kjeborn, R. Schatz, "Design optimization of InGaAsP-InGaAlAs 1.55 μm strain-compensated MQW lasers for direct modulation applications", *Semicond. Sci. Technol.*, **19**, pp. 615-625, 2004.

[2] K. Sato, S. Kuwahara, A. Hirano, M. Yoneyama, Y. Miyamoto, "4 x 40 Gbit/s Dense WDM Transmission over 40-km SMF Using Directly Modulated DFB Lasers", *Proc. of the 30th European Conference on Optical Communication (ECOC2004)*, Stockholm, Sweden, art. no. We1.5.7., 2004.

[3] B. Huiszoon, R.J.W. Jonker, P.K. van Bennekom, G.-D. Khoe, H. de Waardt, "Cost-effective up to 40 Gb/s transmission performance of 1310 nm directly

modulated lasers for short- to medium-range distances", *J. of Lightwave Technol.*, **23**, pp. 1116-1125, 2005.

[4] K. Nakahara, T. Tsuchiya, T. Kitatani, K. Shinoda, T. Taniguchi, T. Kikawa, M. Aoki, M. Mukaikubo, "High Extinction Ratio Operation at 40-Gb/s Direct Modulation in 1.3-μm InGaAlAs-MQW RWG DFB Lasers", *OFC_NFOEC2006, Technical Digest*, art. no OWC5, 2006.

[5] L. Chrostowski, X. Zhao, C. J. Chang-Hasnain, R. Shau, M. Ortsiefer, M.-Ch. Amann, "50 GHz Optically injection-locked 1.55-μm VCSELs", *Photonics Techn. Letters*, **18**, pp. 367-369, 2006.

[6] O. Kjebon, R. Schatz, S. Lourdudoss, S. Nilsson, B. Stalnacke, L. Backborn, "30 GHz direct modulation bandwidth in detuned loaded InGaAsP DBR lasers at 1.55 μm", *IEE Electron. Lett.*, **33**, pp. 488-489, 1997.

[7] L. Bach, W. Kaiser, J.P. Reithmaier, A. Forchel, T.W. Berg, B. Tromborg, "Enhanced direct-modulated bandwidth of 37 GHz by a multi-section laser with a coupled-cavity-injection-grating design", *IEE Electron. Lett.*, **39**, pp. 1592-1593, 2003.

[8] J.P. Reithmaier, W. Kaiser, L. Bach, A. Forchel, M. Gioannini, I. Montroset, T.W. Berg, B. Tromborg, "Modulation speed enhancement by coupling to higher order resonances: a road towards 40 GHz Bandwidth lasers on InP", *Proc. IPRM05*, Glasgow, Scotland, May 8-12, art. no. 05CH37633C, 2005.

[9] U. Feiste, "Optimization of modulation bandwidth of DBR lasers with detuned Bragg reflectors", *IEEE J. of Quantum Electron.*, **34**, pp. 2371-2379, 1998.

[10] G. Morthier, R. Schatz, O. Kjebon, "Extended modulation bandwidth of DBR and external cavity lasers by utilizing a cavity resonance for equalization", *IEEE J. of Quantum Electron.*, **36**, pp. 1468-1475, 2000.

[11] A. Tager, K. Petermann, "High-Frequency Oscillations and Self-Mode Locking in Short External-Cavity Laser Diodes", *IEEE J. of Quantum Electron.*, **30**, pp. 1553-1561, 1994.

[12] H. Wenzel, U. Bandelow, H.-J. Wünsche, J. Rehberg: "Mechanisms of fast self pulsations in two-section DFB lasers", *IEEE J. of Quantum Electron.*, **32**, pp. 69-79, 1996.

[13] O. Brox, S. Bauer, M. Radziunas, M. Wolfrum, J. Sieber, J. Kreissl, B. Sartorius, H.-J. Wünsche: "High-Frequency Pulsations in DFB-Lasers with Amplified Feedback", *IEEE J. of Quantum Electron.*, **39**, pp. 1381-1387, 2003.

[14] S. Bauer, O. Brox, J. Kreissl, B. Sartorius, M. Radziunas, J. Sieber, H.-J. Wünsche, F. Henneberger: "Nonlinear dynamics of semiconductor lasers with active optical feedback", *Phys. Rev. E*, **69**, art. no. 016206, 2004.

[15] M. Radziunas, U. Bandelow, M. Wolfrum, U. Troppenz, J. Kreissl, A. Glitzky, R. Hünlich, "Design of multi-section semiconductor laser for 40 Gb/s direct modulation", *Proc. of the 31th European Conference on Optical Communication (ECOC2005)*, Glasgow, Scotland, art. no. We4.P.088, 2005.

[16] U. Bandelow, M. Radziunas, J. Sieber, M. Wolfrum, "Impact of gain dispersion on the spatio-temporal dynamics of multi-section lasers", *IEEE J. of Quantum Electron.*, **37**, pp. 183-188, 2001.

[17] `LDSL-tool`: "A software package for simulation and analysis of longitudinal dynamics in semiconductor lasers" *http://www.wias-berlin.de/software/ldsl.*

[18] M. Radziunas, "Numerical bifurcation analysis of the traveling wave model of multi-section semiconductor lasers", *Physica D*, **213**, pp. 98-112, 2006.

[19] J. Sieber, "Numerical bifurcation analysis for multi-section semiconductior lasers", *SIAM J. Appl. Dyn. Syst.*, **1**, pp. 248-270, 2002.

[20] `WIAS-TeSCA`: "Two- and three-dimensional semiconductor analysis package" *http://www.wias-berlin.de/software/tesca.*

[21] U. Bandelow, R. Hünlich, T. Koprucki, "Simulation of static and dynamic properties of edge-emitting multiple-quantum-well lasers", *IEEE J. of Sel. Topic in Quant.Electron.*, **9**, pp. 798-806, 2003.